Environmental Pollution 292 (2022) 118266

Contents lists available at ScienceDirect

Environmental Pollution

journal homepage: www.elsevier.com/locate/envpol

Estimating organic aerosol emissions from cooking in winter over the Pearl River Delta region, China☆

Li Xing [a,*], Tzung-May Fu [b,c], Tengyu Liu [d,1], Yiming Qin [e], Liyuan Zhou [d], Chak K. Chan [d], Hai Guo [f], Dawen Yao [f], Keqin Duan [a]

[a] School of Geography and Tourism, Shaanxi Normal University, Xi'an, Shaanxi, China
[b] State Environmental Protection Key Laboratory of Integrated Surface Water-Groundwater Pollution Control, School of Environmental Science and Engineering, Southern University of Science and Technology, Shenzhen, Guangdong, China
[c] Shenzhen Institute of Sustainable Development, Southern University of Science and Technology, Shenzhen, Guangdong, China
[d] School of Energy and Environment, City University of Hong Kong, Hong Kong, China
[e] School of Engineering and Applied Sciences, Harvard University, Cambridge, MA, United States
[f] Department of Civil and Environmental Engineering, The Hong Kong Polytechnic University, Hong Kong, China

ARTICLE INFO

Keywords:
WRF-Chem
Cooking organic aerosol
Pearl river delta region
Emissions

ABSTRACT

Cooking is an important source of organic aerosols (OA), particularly in urban areas, but it has not been explicitly included in current emission inventories in China. This study estimated the organic aerosol emissions from cooking during winter over the Pearl River Delta (PRD) region, China. Using the retrieved hourly cooking organic aerosol (COA) concentrations at two sites in Hong Kong and Guangzhou, population density, and daily per capita COA emissions, we determined the spatial and temporal distribution of COA emissions over the PRD region based on two approaches by treating COA as non-volatile (NVCOA) and semi-volatile (SVCOA), respectively. By using the estimated COA emissions and the Weather Research and Forecasting model coupled with chemistry (WRF-Chem) model, we reproduced the diurnal cycles of COA concentrations at the PolyU site in Hong Kong and Panyu site in Guangzhou. We also resolved the different patterns of COA between weekdays and weekends. The mean COA concentration during wintertime over the urban areas of the PRD region was 0.7 μg m^{-3} and 0.9 μg m^{-3} for the NVCOA and SVCOA cases, respectively, contributing 5.1% and 6.9% to the urban OA concentrations. The total COA emissions in winter over the PRD region were estimated to be 3.5×10^8 g $month^{-1}$ and 3.8×10^8 g $month^{-1}$ for the NVCOA and SVCOA cases, respectively, adding 34.8% and 37.8% to the total primary organic aerosol emissions. Considering COA emissions in the model increased the mean regional OA concentrations by 4.6% and 7.4% for the NVCOA and SVCOA cases, respectively. Our study therefore highlights the importance of cooking activities to OA concentrations in winter over the PRD region.

1. Introduction

Organic aerosol (OA) is an important component of $PM_{2.5}$, constituting a large fraction of its mass worldwide (Zhang et al., 2007; Jimenez et al., 2009). Two types of OA are usually used to represent different OA formation pathways, namely primary OA (POA) with direct emissions from various combustion sources, and secondary OA (SOA) formed through various oxidation pathways in the atmosphere (Hallquist et al., 2009; Zhang et al., 2011; Zhou et al., 2020). The radiative balance, cloud properties, and precipitation could be influenced by OA via absorbing or scattering the solar radiation, and acting as cloud condensation nuclei and ice nuclei (IPCC, 2013). High OA concentrations are also harmful to human health (Yan et al., 2019). Reliable OA emission inventories are of vital importance for evaluating the climatic and human effects of OA, and could also provide important information for source apportionment of OA.

In China, chemical transport models for OA simulations have been improved significantly in recent years, but most model results continue to underestimate the observed OA concentrations (Fu et al., 2012; Li et al., 2013; Feng et al., 2016; Hu et al., 2017; Miao et al., 2020). The

☆ This paper has been recommended for acceptance by Admir C. Targino.

* Corresponding author.
E-mail address: xingli@snnu.edu.cn (L. Xing).

[1] Now at: School of Atmospheric Sciences, Nanjing University, Nanjing, Jiangsu, China.

https://doi.org/10.1016/j.envpol.2021.118266
Received 11 May 2021; Received in revised form 9 September 2021; Accepted 29 September 2021
Available online 2 October 2021

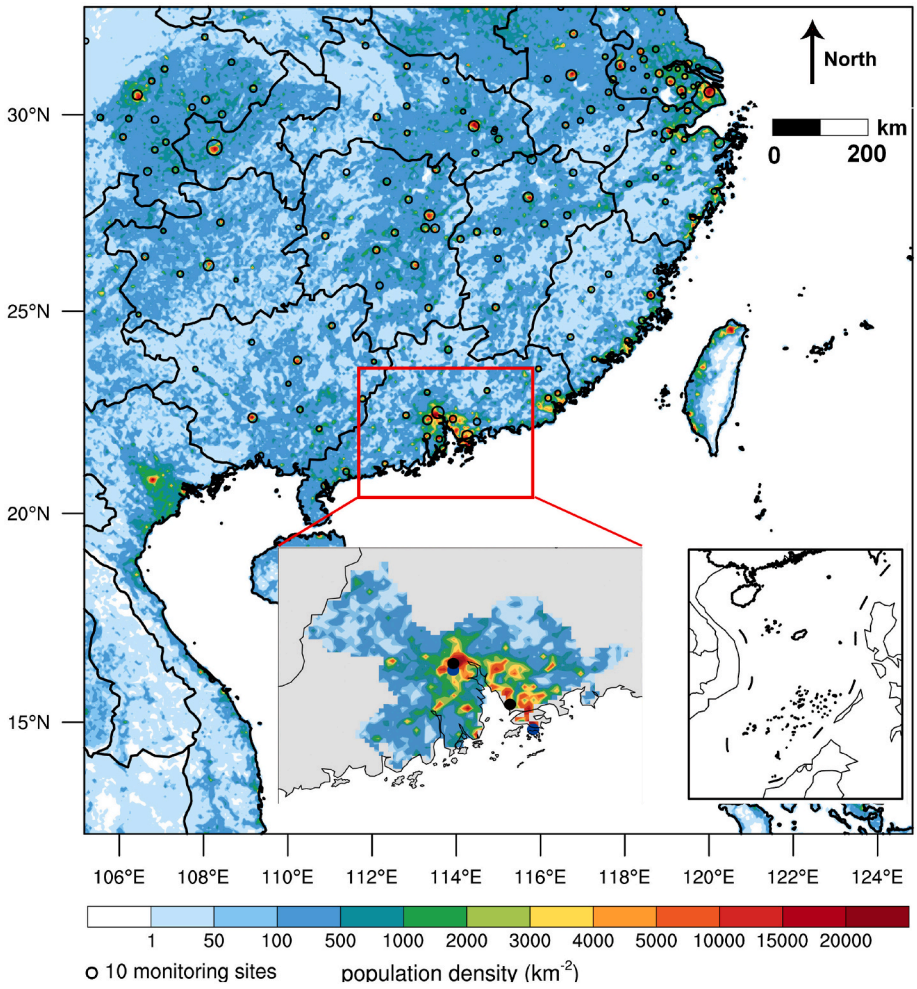

Fig. 1. WRF-Chem model domain with the population density. The black hollow circles denote the centers of cities that have ambient monitoring sites, and the sizes of the circles denote the number of ambient monitoring sites in the cities. The inset shows the population density in the PRD region. The two blue circles in the inset represents the location of the urban roadside site at the Hong Kong Polytechnic University (PolyU) (22.30 °N, 114.18 °E) and Panyu Atmospheric Composition station at Guangzhou (Panyu) (23.00 °N, 113.21 °E). The two black circles in the inset represent the locations of two urban sites in Shenzhen (22.6 °N, 113.9 °E) and Guangzhou (23.08 °N, 113.21 °E). (For interpretation of the references to colour in this figure legend, the reader is referred to the Web version of this article.)

underestimation has been shown to originate from under-predicted SOA formation, or misrepresented or missing sources of POA in the emission inventories. One missing primary source of POA in emission inventories is cooking (Zheng et al., 2018).

Using aerosol mass spectrometer (AMS) measurements with positive matrix factorization (PMF) analyses, several studies have reported that cooking OA (COA) is an important component of OA worldwide and contribute 10%–35% to the total OA mass (Allan et al., 2010; Sun et al., 2011, 2018; Mohr et al., 2012; Crippa et al., 2013; Xu et al., 2015), although the AMS measurement might likely overestimate COA concentrations (Reyes-Villegas et al., 2018; Katz et al., 2021). In China, the contributions of COA to OA in winter were found to be relatively higher during non-haze days (9.3%–11.5%), compared with those during haze days (3.6%–5.8%) (Elser et al., 2016). In the Pearl River Delta (PRD) region in southern China, the mass fractions of COA in OA were higher in urban areas (20.6%–34.6%) than those in the rural areas (6.5%–9.6%) (Lee et al., 2015; Qin et al., 2017; Cao et al., 2018; Yao et al., 2021).

Cooking emissions are affected by various factors, such as cooking style, oils, food ingredients, temperature, and duration (Wang et al., 2017). Using the retrieved COA concentrations and population density in Paris, Fountoukis et al. (2016) used a three-dimensional regional chemical transport model (PMCAMx) to simulate the COA concentrations, and estimated the COA emissions in Paris to be ~80 mg day^{-1} person^{-1}. The COA emissions in the UK were estimated to be 320 mg day^{-1} person^{-1} and the annual COA emissions to be 7.4 Gg year^{-1}, adding 10% to the national anthropogenic $PM_{2.5}$ emissions in 2012 (Ots et al., 2016). Chinese-style cooking is popular worldwide because of its versatile food ingredients, special seasoning, and cooking style, and results in different emissions compared with western-style cooking (He et al., 2004). To the best of our knowledge, there have been lack of COA emission estimations in China.

The PRD region is highly populated and one of the largest economic regions in China. Although $PM_{2.5}$ concentrations in the PRD region have declined in recent years due to emission control strategies (Zhai et al., 2019), COA emissions could potentially be important emission sources due to the high population density in the PRD region. Ye et al. (2019) showed that Guangzhou, in the PRD region, was one of the four most populous cities in mainland China. The population density in Hong Kong was also very high with about 6777 people km^{-2} on average (Hua et al., 2021).

In this study, we used the AMS-retrieved COA concentrations in Hong Kong and Guangzhou and the population density data from the LandScan database to produce gridded COA emissions in the PRD region (Dobson et al., 2000; Qin et al., 2017; Liu et al., 2019). We added a COA tracer in the Weather Research and Forecasting Model coupled with Chemistry (WRF-Chem) model, and simulated COA concentrations in the PRD region with the updated emission inventory for COA. The simulated COA concentrations were compared with observations in Hong Kong and Guangzhou by conducting different sensitivity tests with respect to the emission inventories, until the model could capture the diurnal cycles of observed COA concentrations. The model results were then validated with observed COA concentrations at two other sites in Shenzhen and Guangzhou. Finally, the total winter COA emissions in the PRD region and the effect of COA on the OA concentrations were evaluated.

2. Methods

2.1. Model description

We used the WRF-Chem model developed by Li et al. (2011). The model utilized the gas-phase chemical mechanism "Statewide Air Pollution Research Center-99" (SAPRC-99), and the aerosol module from the "Community Multi-scale Air Quality Model" (CMAQ)/Model 3 (Binkowski and Roselle, 2003). A volatility basis set (VBS) approach with aging was used to simulate OA (Li et al., 2011; Xing et al., 2019). Nine surrogate species with saturation concentrations (C^*) ranging from 10^{-2} to 10^{6} μg m^{-3} were used to represent the semi-volatile POA components emitted from the traffic-related emission and biomass burning and the fraction of POA emissions for each surrogate species were assigned based on the results in Tsimpidi et al. (2010). They were assumed to be oxidized by OH with a rate constant of 2×10^{11} cm^3 $molec^{-1}$ s^{-1} to form the species with reduced volatility of one order of magnitude and increased the mass by 7.5% due to the added oxygen. SOA formed from each anthropogenic or biogenic precursor was calculated by four semi-volatile VOCs with saturation concentrations of 1, 10, 100, 1000 μg m^{-3} and the SOA yields were applied from the results in Tsimpidi et al. (2010). The heterogeneous reactions glyoxal and methylglyoxal from primary emissions and secondary formation on aerosol surfaces to form SOA were also included in the model. The COA concentrations could not be predicted using the WRF-Chem model because this model did not include the chemical species of COA. Moreover, COA emissions were not included in the current widely-used Multi-resolution Emission Inventory for China (MEIC) (Zheng et al., 2018).

Here, a COA tracer was incorporated into the WRF-Chem model. Previous studies revealed that COA was semi-volatile and could undergo further photochemical reactions, contributing to SOA formation (Liu et al., 2017, 2018a, b; Louvaris et al., 2017; Takhar et al., 2019, 2021; Zhang et al., 2020), but the volatility distributions of COA varied significantly for different cooking oils and experimental conditions (Louvaris et al., 2017; Takhar et al., 2019). Two approaches for COA were applied in the model. For the NVCOA case serving as the base simulation, the COA tracer was assumed to be non-volatile and did not evolve chemically, but was incorporated into the total OA mass for the calculation of absorptive partitioning of SOA (Ots et al., 2016). For the SVCOA case serving as the sensitivity simulation, COA was treated as semi-volatile and the volatility distribution followed the results from canola oil oxidized by OH in Takhar et al. (2019). They were oxidized by OH with a rate constant of 2×10^{11} cm^3 $molec^{-1}$ s^{-1} to form the species with reduced volatility of one order of magnitude and increased the mass by 7.5% due to the added oxygen.

Fig. 1 shows the model domain, which included 400 × 400 grid cells with the horizontal resolution of 6 km and 35 vertical model layers. The parameterization schemes for different processes, including the microphysics, longwave and shortwave radiation, the land-surface model, the surface layer, and boundary layer scheme were the same as Xing et al. (2020). The meteorological and chemical initial and boundary conditions used the National Centers for Environmental Prediction (NCEP) 1° × 1° reanalysis data (https://rda.ucar.edu/datasets/ds083.2/) and the model output from the Model for OZone And Related chemical Tracers (MOZART) with 6 h intervals (Horowitz et al., 2003). To estimate COA emissions in winter over the PRD region, we simulated the OA and $PM_{2.5}$ concentrations from December 27, 2017 to January 15, 2018. The spin-up time was 2 days.

The anthropogenic emission inventory of MEIC, including the agricultural, industrial, power plant, residential, and transportation sectors with the base year of 2016, was used in the simulation (Zhang et al., 2009; Zheng et al., 2018). The Fire Inventory from the National Center for Atmospheric Research in US (FINN) was employed for the biomass burning emissions (Wiedinmyer et al., 2006, 2011). The FINN inventory included the open burning of wildfire, agricultural fires and managed burning, but did not include the biofuel use and trash burning. The biogenic emissions were calculated online from the Model of Emissions of Gases and Aerosols from Nature (MEGAN) module (Guenther et al., 2006).

2.2. Observation data

The OA was measured at an urban roadside site at the Hong Kong Polytechnic University (PolyU) (22.30 °N and 114.18 °E) from December 27, 2017 to January 15, 2018 and Panyu Atmospheric Composition station in Guangzhou (Panyu) (23.00 °N, 113.21 °E) from November 7, 2014 to January 3, 2015 using a high-resolution time-of-flight aerosol mass spectrometer (HR-ToF-AMS, Aerodyne Research Incorporated, Billerica, MA). Details of the measurements are described in Qin et al. (2017), Liu et al. (2019), and Yao et al. (2021). The HR-ToF-AMS was operated with the high sensitivity V-mode and high resolution W-mode to get the mean particle mass spectra every 5 min, and the relative ionization efficiency for different species were calibrated. We calculated the hourly mean data for model validation. The PolyU site is located less than 1 km in the east of the Tsim Sha Tsui commercial areas with a large number of restaurants, and in the west and southwest of the residential areas with numerous buildings and restaurants (Yao et al., 2021). The Panyu site is surrounded by residential neighborhoods (Qin et al., 2017). The contributions of COA to OA for both sites were significant (25.4 ± 0.3% at the PolyU site and 6.5%–9.6% at the Panyu site) due to the intensive emissions.

To evaluate the model performance, the measured hourly $PM_{2.5}$ and NO_2 concentrations over the model domain were downloaded from the website of China's Ministry of Ecological Environment (http://www.aqistudy.cn/). The monitoring sites are shown in Fig. 1.

2.3. OA source apportionment

Positive matrix factorization (PMF) analysis was employed to the mass spectra from the AMS measurement to resolve the different OA factors (Qin et al., 2017; Liu et al., 2019). For the PolyU site, five factors were identified, including two primary emission-dominated factors (hydrocarbon-like OA (HOA) and COA), and three oxygenated factors (OOA1, OOA2, and OOA3) associated with different oxidation levels. For the Panyu site, the resolved OA factors included three primary-dominated factors (HOA, COA, biomass-burning-related OA (BBOA)), and two oxygenated factors (SVOOA and LVOOA). We used the analyzed COA concentrations for the PolyU and Panyu sites to validate model results and estimate COA emissions.

The diurnal profiles of COA concentrations at two urban sites in Shenzhen (113.90 °E, 22.60 °N) and Guangzhou (113.21 °E, 23.08 °N) in winter, respectively (Cao et al., 2018; Guo et al., 2020) were used to evaluate the simulated COA concentrations at the two sites based on the estimated COA emissions.

2.4. Estimation of COA emissions

The COA emissions over the model domain were estimated using population density and observed diurnal profiles of COA concentrations at the PolyU and Panyu sites following the method from Ots et al., (2016). Fig. 1 shows the population density for 2017 from the LandScan dataset. We estimated the spatiotemporal distribution of COA emissions based on the population density, observed diurnal profiles of COA concentrations at the PolyU and Panyu sites on the assumption that the daily per capita cooking emission value was 320 mg day^{-1} $person^{-1}$ (Ots et al., 2016). We then compared the simulated COA concentrations from the NVCOA and SVCOA simulations with the observations at the PolyU and Panyu sites. Based on the difference of simulated and observed COA concentrations at the PolyU and Panyu sites, we adjusted the daily per capita cooking emission value and hourly COA emission percentages multiple times, until the model could reproduce the magnitude and

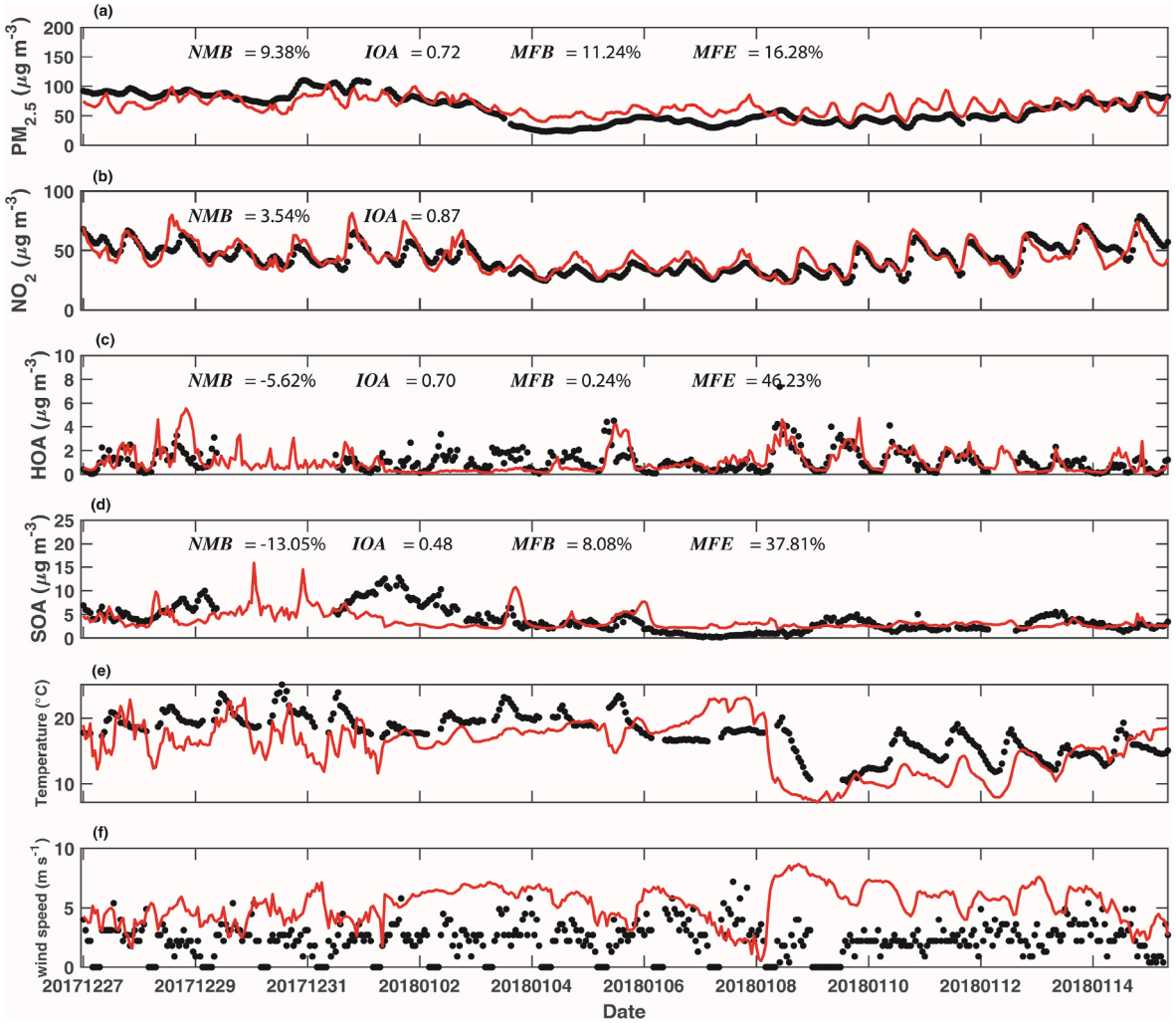

Fig. 2. Comparisons of observed (black dots) and simulated (red lines) temporal variations of (a) $PM_{2.5}$ concentrations and (b) NO_2 averaged at the ambient monitoring sites, (c) HOA concentrations, (d) SOA concentrations, (e) Temperature, and (f) wind speed at the PolyU site from December 27, 2017 to January 15, 2018. (For interpretation of the references to colour in this figure legend, the reader is referred to the Web version of this article.)

variations of observed COA concentrations at the PolyU and Panyu sites.

2.5. Statistical indexes for model evaluation

We employed four numerical metrics to evaluate model results: the normalized mean bias (*NMB*), index of agreement (*IOA*), mean fractional bias (*MFB*), and mean fractional error (*MFE*).

$$NMB = \frac{\frac{1}{N}\sum_{i=1}^{N}(P_i - O_i)}{\overline{O}} \times 100\% \quad (1)$$

$$IOA = 1 - \frac{\sum_{i=1}^{N}(P_i - O_i)^2}{\sum_{i=1}^{N}(|P_i - \overline{O}| + |O_i - \overline{O}|)^2} \quad (2)$$

$$MFB = \frac{1}{N}\sum_{i=1}^{N}\frac{(P_i - O_i)}{(O_i + P_i/2)} \quad (3)$$

$$MFE = \frac{1}{N}\sum_{i=1}^{N}\frac{|P_i - O_i|}{(O_i + P_i/2)} \quad (4)$$

where P_i and O_i represent the simulated and observed concentrations of the chemical species i, respectively, N is the number of model and observation data used for comparisons, $\overline{O}$ is the mean observed concentration, and *IOA* represents the level of consistency between the model and the observation. *MFB* and *MFE* were used for the particulate matter validation of model performance. The model performance goal was set to be met when both the *MFB* and *MFE* were lower than ±30% and +50%, respectively. The MFB ≤75% and MFE ≤60% also met the model performance criteria for less abundant species, as they had less stringent goals and criteria for model evaluation (Boylan and Russell, 2006).

3. Results and discussion

3.1. Model validation

Fig. 2a and Fig. 2b show the temporal variations of the simulated and observed $PM_{2.5}$ and NO_2 concentrations averaged over all monitoring sites in the model domain, respectively. The model generally reproduced the temporal change of $PM_{2.5}$ concentrations, but predicted more distinct variations than those of the observations. The *NMB* and *IOA* were 9.38% and 0.72, respectively. The *MFB* and *MFE* for $PM_{2.5}$ were 11.24% and 16.28%, which were acceptable for model performance (Boylan and Russell, 2006). The model also reproduced the temporal variation of NO_2 concentrations, with *NMB* and *IOA* to be 3.54% and 0.87, respectively, showing a good representation of NO_2 emission in the MEIC emission inventory over the model domain.

Fig. 2c and Fig. 2d present the temporal variations of the simulated

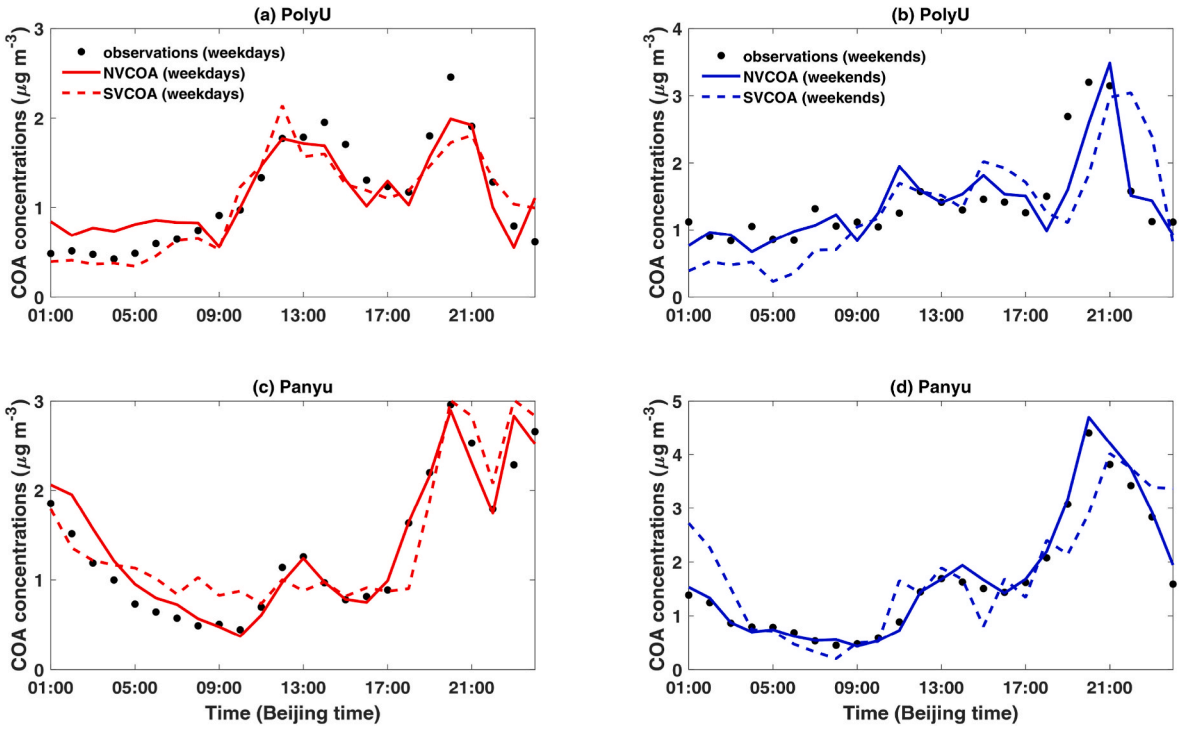

Fig. 3. The diurnal cycles of observed (black dots) and simulated (red and blue lines) COA concentrations on weekdays ((a) PolyU site and (c) Panyu site) and weekends ((*b*) PolyU site and (d) Panyu site). The solid and dashed lines denote the NVCOA and SVCOA cases, respectively. (For interpretation of the references to colour in this figure legend, the reader is referred to the Web version of this article.)

and observed HOA and SOA concentrations at the PolyU site. The model reproduced the diurnal variations of HOA at the PolyU site, particularly from January 4 to 15, 2018 (Fig. 2c). The HOA was mainly associated with traffic emissions and showed a distinct peak during the morning rush hours, while the HOA concentrations during the evening rush hours were not as high as that of the morning rush hours. The *NMB* and *IOA* for HOA were −5.62% and 0.70, respectively. The *MFB* and *MFE* for HOA at the PolyU site were 0.24% and 46.23%, which met the criteria for the acceptance for model performance (Boylan and Russell, 2006). The model simulated the relatively high-observed SOA concentrations during the first half of the simulation periods, and the relatively low SOA concentrations during the later periods (Fig. 2d). The SOA simulation results were inferior to those of HOA, with *NMB* and *IOA* to be −13.05% and 0.48, respectively. The *MFB* and *MFE* for SOA at the PolyU site were 8.08% and 37.81%, which were also acceptable for model performance (Boylan and Russell, 2006). Fig. 2e and Fig. 2f presented the observed and simulated near-surface temperature and wind speed at the PolyU site. The model generally reproduced the temporal variations of temperature at the PolyU site and captured the sharp cooling on January 8, 2018, but the model tended to underestimate the near-surface temperature during most time of the simulation period. The model slightly overestimated the observed wind speed at the PolyU site for most of the time, partly caused by the coarse horizontal resolution of 6 km. The PolyU site is located less than 1 km from the Victoria Harbor and there are both sea and land within the 3 km circle of the PolyU site, but the model could not resolve the difference surrounding the site.

3.2. Diurnal cycles of COA

We further explored the diurnal variations of COA at the PolyU and

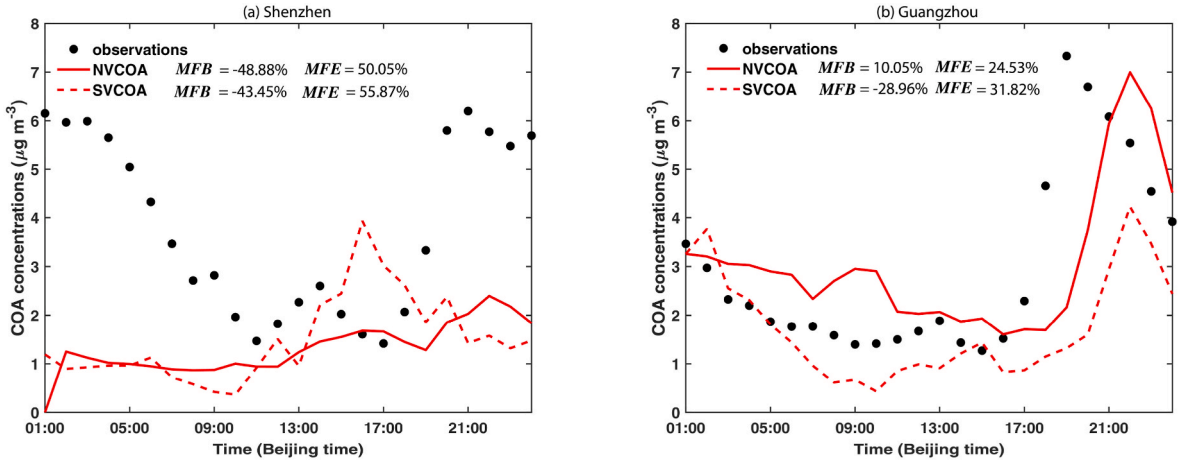

Fig. 4. The diurnal variations of observed (black dots) and simulated (solid line: NVCOA, dashed line: SVCOA) COA concentrations at (a) Shenzhen and (b) Guangzhou.

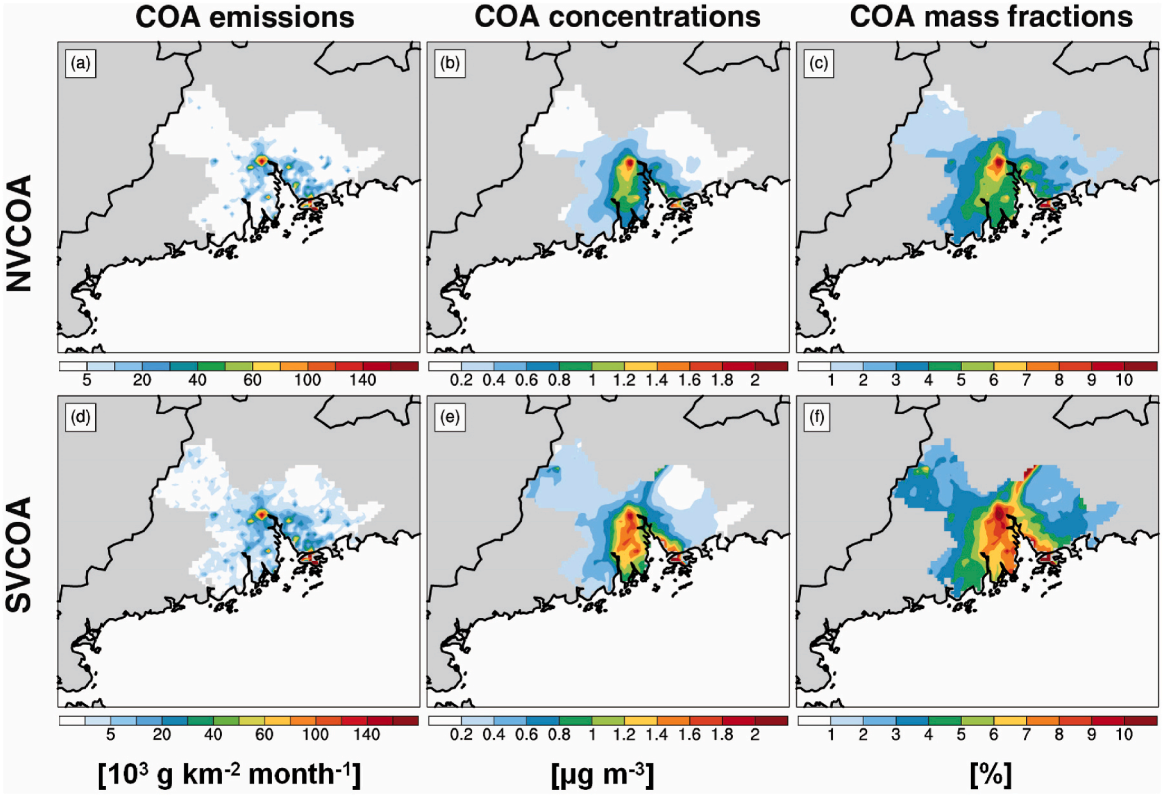

Fig. 5. The spatial distributions of (a, c) COA emissions, (b, e) COA concentrations, and (c, f) COA mass fractions to OA over the PRD region averaged from December 27, 2017 to January 15, 2018. The top and bottom panels denote the results from the NVCOA and SVCOA cases, respectively. The data outside the PRD region are not shown.

Panyu sites on weekdays and weekends. The observed COA concentrations on the weekdays had two distinct peaks during lunchtime (12:00–14:00 local time) and dinnertime (19:00–21:00 local time) for both the PolyU and Panyu sites, with maximum concentrations of 2.0 and 1.3 μg m^{-3} during lunchtime and 2.5 and 3.0 μg m^{-3} during dinnertime, respectively (Fig. 3a and Fig. 3c). The relatively high ratio of COA concentrations during lunchtime over that during dinnertime at the PolyU site indicated that the PolyU site was close to commercial areas with large COA emissions from restaurants during lunchtime and dinnertime, while the relatively low ratio at the Panyu site reflected that the Panyu site was surrounded by the residential areas with low COA emissions from family cooking during lunchtime. The observed weekend COA concentrations presented one peak during dinnertime, with a maximum concentration of 3.2 and 4.4 μg m^{-3} (Fig. 3b and Fig. 3d), which were significantly higher than that on weekdays, while the COA concentrations during lunchtime on weekends did not show an obvious increase. The daily mean COA concentration during weekends was 1.4 μg m^{-3} and 1.6 μg m^{-3} for the PolyU and Panyu sites, which were higher than those of 1.1 μg m^{-3} and 1.3 μg m^{-3} on weekdays. The model simulations for both the NVCOA and SVCOA cases were fitted to capture the diurnal variations of COA on weekdays and weekends for the PolyU and Panyu sites.

To further validate the estimated COA emissions, we compared the simulated COA concentrations with observations at two urban sites in Shenzhen (113.90 °E, 22.60 °N) and Guangzhou (113.21 °E, 23.08 °N) in winter, respectively (Cao et al., 2018; Guo et al., 2020). Fig. 4a showed that the model generally underestimated the observed COA concentrations in Shenzhen for the whole day, except that the SVCOA case overestimated the COA concentrations during dinnertime. The *MFB* and *MFE* for COA at the Shenzhen site were −48.88% and 50.05% for the NVCOA case, while the *MFB* and *MFE* for the SVCOA case were −43.45% and 55.87%, respectively. The model performance at the Shenzhen site met the model performance criteria. Fig. 4b showed that the model generally captured the diurnal variations of COA concentrations at the Guangzhou site, and the simulated COA concentrations for the SVCOA case were lower than those from the NVCOA case. The simulated contribution of COA to OA were 20.8% and 14.8% for the NVCOA and SVCOA cases, respectively, which were comparable with the observed OA mass fractions of 18% (Guo et al., 2020). The *MFB* and *MFE* for COA at the Guangzhou site were 10.05% and 24.53% for the NVCOA case, and −28.96% and 31.82% for the SVCOA case, respectively, which met the model performance criteria for less abundant species. In conclusion, the model performance for the COA simulation in Shenzhen and Guangzhou was acceptable, and the model results were useful for estimating COA emissions over the PRD region.

3.3. Hourly and spatial distributions of COA emissions

Based on the minimal difference between the simulated and observed COA concentrations at the PolyU and Panyu sites, the best estimation of daily per capita COA emissions over the PRD region on weekends were 209 mg day^{-1} $person^{-1}$ and 152 mg day^{-1} $person^{-1}$ for the NVCOA and SVCOA case, respectively, while they were 149 mg day^{-1} $person^{-1}$ and 190 mg day^{-1} $person^{-1}$ on weekdays. The daily per capita COA emissions over the PRD region were lower than that in the UK (Ots et al., 2016), but higher than that in France (Fountoukis et al., 2016). This was probably caused by the differences in cooking styles. The most popular Cantonese cooking style in the PRD region is usually frying, stewing, or braising, while in the UK it is grilling, frying, or even deep-frying, all of which produce higher OA emissions (Ots et al., 2016). Figure S1 shows the diurnal variations of COA emission percentages on weekdays and weekends in the PRD region. The diurnal cycles of COA emission percentages for the NVCOA and SVCOA cases were similar, except that the variations for the NVCOA case were smaller than those

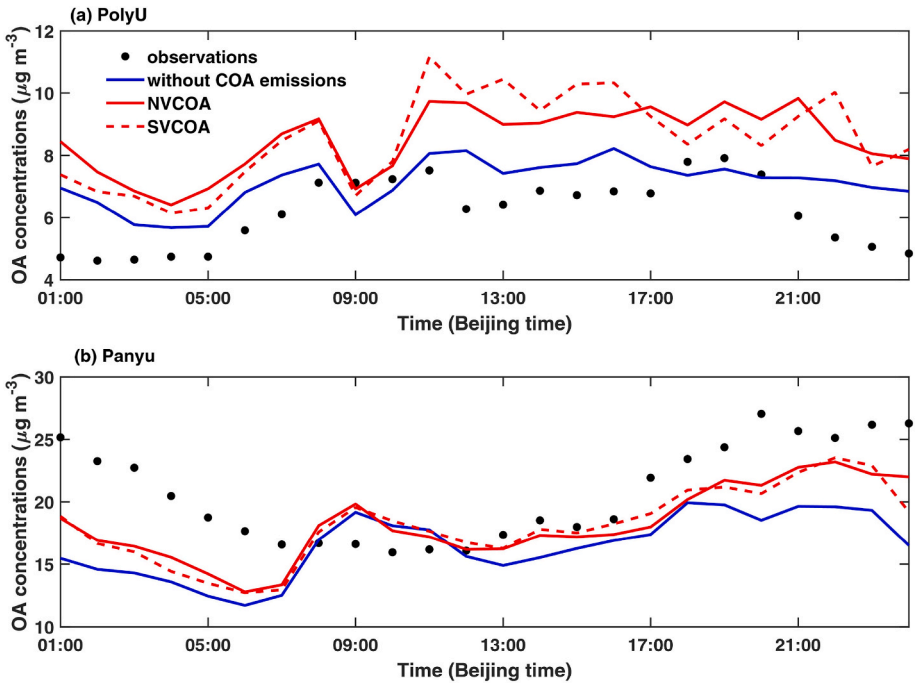

Fig. 6. The diurnal cycles of observed (black dots) and simulated (blue lines: without COA emissions, red solid lines: NCVOA, red dashed lines: SVCOA) OA concentrations at the (a) PolyU site and (b) Panyu site. (For interpretation of the references to colour in this figure legend, the reader is referred to the Web version of this article.)

for the SVCOA case. For the NVCOA case, COA emission percentages during dinnertime were the highest on both weekdays and weekends, accounting for 31.8% and 28.3% of total daily COA emissions on weekdays and weekends, respectively. The COA emission percentages during lunchtime were 24.4% and 24.5% on weekdays and weekends, respectively. The COA emissions between the lunchtime and dinnertime were much higher on weekends than those on weekdays, reflecting that people have more casual time for eating on weekends, higher background concentrations of COA, and/or more emissions from restaurant dining than those during weekdays.

Fig. 5 demonstrates the spatial distributions of the estimated COA emissions, modeled COA concentrations, and COA mass fractions to OA for the NVCOA and SVCOA cases averaged over the simulation period in the PRD region. The high COA emissions (exceeding 30.0×10^3 g km^{-2} month^{-1}) originated in the central areas of the PRD region due to the high population density, particularly in the city centers, with emissions higher than 80×10^3 g km^{-2} month^{-1} (Fig. 5a and 5d). The COA emissions in the marginal areas of the PRD region were significantly lower and generally did not exceed 10.0×10^3 g km^{-2} month^{-1}. The total COA emissions in winter over the PRD region were estimated to be 3.5×10^8 g month^{-1} for the NVCOA case and 3.8×10^8 g month^{-1} for the SVCOA case. The total primary organic carbon emissions in winter over the PRD region from the MEIC emission inventory were 6.1×10^8 g month^{-1} (Zheng et al., 2018). The COA emissions based on the NVCOA and SVCOA cases added 34.8% and 37.8% to the total primary OA emissions (multiplied by OM/OC ratio of 1.65) (Xing et al., 2013), thereby making up an important source of primary OA during wintertime over the PRD region. The simulated COA concentrations were also at a high level in the central area of the PRD region (Fig. 5b and 5e). The COA emissions and concentrations in Guangzhou were the highest over the PRD region, exceeding 160.0×10^3 g km^{-2} month^{-1} and 2.0 μg m^{-3}, respectively. Unlike the relatively high COA emissions in Dongguan, Shenzhen, and Hong Kong, that are located in the southeast of Guangzhou, the simulated COA concentrations in Foshan, Zhongshan, and Zhuhai in the southwest of Guangzhou were higher than those in the southeast of Guangzhou. The simulated COA concentrations and mass fractions from the SVCOA case were higher than those from the NVCOA case. The land-use data in 2018 from the remote sensing images of Landsat 8 was used to identify the urban areas in the PRD region (http://www.resdc.cn, Figure S2). On the daily average in the urban areas of the PRD region in winter, the COA concentration was 0.7 μg m^{-3} and 0.9 μg m^{-3} for the NVCOA and SVCOA cases, respectively, contributing 5.1% and 6.9% to the urban OA concentrations. The COA concentration and contribution to OA in the urban areas were significantly higher than those of 0.35 μg m^{-3} and 3.2% contribution for the NVCOA case and 0.51 μg m^{-3} and 4.7% contribution for the SVCOA case over the entire PRD region.

3.4. The impact of COA emissions on SOA concentrations

Since COA was incorporated into the total OA mass for the absorptive partitioning of POA and SOA, the added COA emissions would affect the OA concentrations over the PRD region. We evaluated the impact of COA emissions on OA concentrations by conducting a sensitivity simulation turning off the COA emissions. Fig. 6 shows the diurnal variations of observed and simulated OA concentrations at the PolyU and Panyu sites. Fig. 6a shows that OA concentrations at the PolyU site in the morning and afternoon were relatively high and could be up to 7.0 μg m^{-3}, while the OA concentrations at night were the lowest (4.6 μg m^{-3}). The model generally captured the diurnal profile of OA concentrations at the PolyU site, but tended to overestimate OA concentrations for all three simulations. On the daily average, considering COA emissions in the model increase OA concentrations at the PolyU site by 1.4 μg m^{-3} for both the NVCOA and SVCOA cases. Fig. 6b presents that OA concentrations at the Panyu site were high at night and low during daytime. The model reproduced the diurnal profile of OA concentrations at the Panyu site, although it overestimated OA concentrations in the morning. Considering COA emissions increased the OA concentrations at the Panyu site by 1.7 μg m^{-3} for the NVCOA case and 1.6 μg m^{-3} for the SVCOA case, respectively. Considering COA emissions led to better agreement between the model and observations, with *IOA* increased from 0.53 for the case without COA emissions to 0.73 for the NVCOA

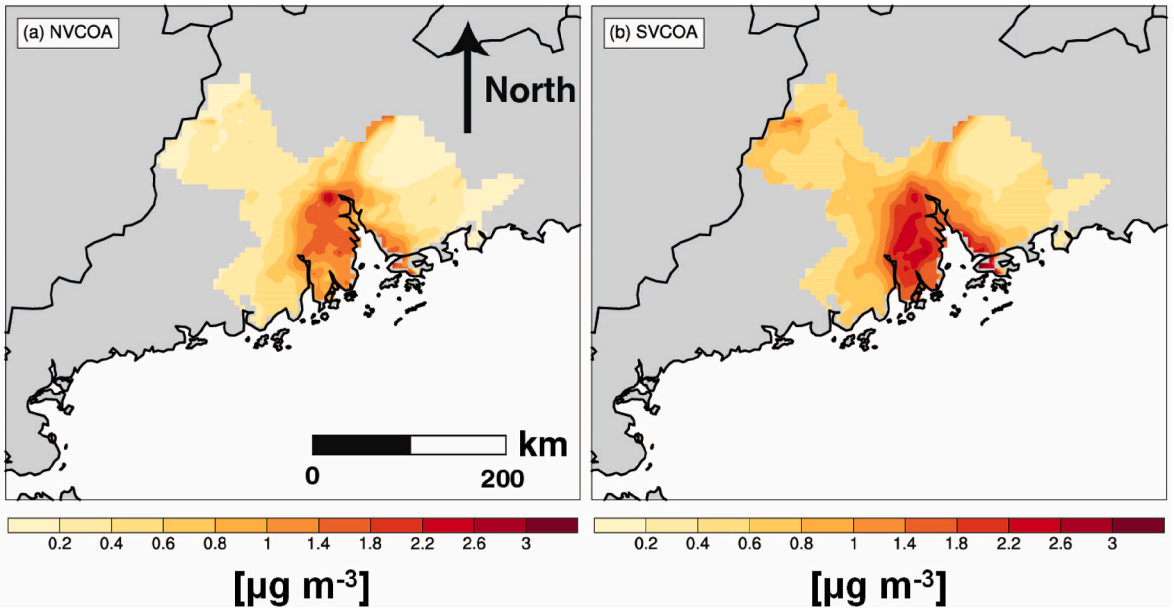

Fig. 7. The spatial distribution of OA concentration changes due to the inclusion of COA emissions in the WRF-Chem model from (a) NVCOA and (b) SVCOA cases averaged from December 27, 2017 to January 15, 2018. The data outside the PRD region are not shown.

case and 0.68 for the SVCOA case.

Fig. 7 presents the effect of COA emissions on OA concentrations averaged from December 27, 2017 to January 15, 2018. Including COA emissions in the model enhanced OA concentrations over the whole PRD region by 0–3 μg m^{-3} and the enhancement was higher from the SVCOA case than that from the NVCOA case. On the regional average, considering COA emissions in the model increased OA concentrations by 0.5 μg m^{-3} for the NVCOA case and 0.8 μg m^{-3} for the SVCOA case, respectively, enhancing 4.6% and 7.4% of the total OA mass.

4. Conclusions

In this study, COA emissions were estimated during winter over the PRD region using two approaches assuming COA to be non-volatile and semi-volatile, respectively. The best estimation of COA emissions in winter over the PRD region was 3.5 × 10^8 g $month^{-1}$ for the NVCOA case and 3.8 × 10^8 g $month^{-1}$ for the SVCOA case, adding 34.8% and 37.8% to the total primary OA emissions. The results indicate that COA emissions over the PRD region during winter are important primary OA sources. The mean COA concentration during winter over the urban areas of PRD region was 0.7 μg m^{-3} and 0.9 μg m^{-3} for the NVCOA and SVCOA cases, contributing 5.1% and 6.9% to the total OA concentrations. Considering COA emissions in the model increased the simulated OA concentrations by 4.6% and 7.4% to the total OA concentrations on the PRD regional average, which would potentially play an important role for narrowing the gap between the model and observed OA concentrations.

The estimated higher COA emissions, higher COA concentrations, and higher enhancement for OA concentrations based on the SVCOA case than those from the NVCOA case indicated the importance for treating COA as semi-volatile in the model. Given that laboratory studies have shown that VOCs from cooking also contribute to SOA formation and the volatility distributions of COA from different cooking activities may vary significantly, further studies are needed to parameterize the aging rates and SOA formation from primary COA emissions, so that the model can accurately simulate both POA and SOA concentrations from cooking activities.

Credit author statement

Li Xing: Conceptualization, Methodology, Software, Visualization, Writing – original draft. **Tzung-May Fu**: Conceptualization, Supervision, Writing – review & editing. **Tengyu Liu**: Data curation, Resources. **Yiming Qin**: Data curation, Resources. **Liyuan Zhou**: Data curation, Writing – review & editing. **Chak K. Chan**: Funding acquisition, Writing – review & editing. **Hai Guo**: Resources, Writing – review & editing. **Dawen Yao**: Writing – review & editing. **Keqin Duan**: Supervision.

Declaration of competing interest

The authors declare that they have no known competing financial interests or personal relationships that could have appeared to influence the work reported in this paper.

Acknowledgements

This study is supported by the National Natural Science Foundation of China (Grant nos. 41807310), the Natural Science Foundation of Shaanxi Province (2020JQ-414), the Fundamental Research Funds for the Central Universities (GK202003066), the Guangzhou Development District International Science and Technology Cooperation Project (No. 2018GH08), and ECF Environmental and Conservation Fund (Project 7/2020). We acknowledge the help of Dr. Xin Long and Dr. Jianwu Yan for processing the LandScan data and Dr. Guohui Li for helpful discussion.

Appendix A. Supplementary data

Supplementary data to this article can be found online at https://doi.org/10.1016/j.envpol.2021.118266.

References

Allan, J.D., Williams, P.I., Morgan, W.T., Martin, C.L., Flynn, M.J., Lee, J., Nemitz, E., Phillips, G.J., Gallagher, M.W., Coe, H., 2010. Contributions from transport, solid fuel burning and cooking to primary organic aerosols in two UK cities. Atmos. Chem. Phys. 10, 647–668.

Binkowski, F.S., Roselle, S.J., 2003. Models-3 community multiscale air quality (CMAQ) model aerosol component –1. Model description. J. Geophys. Res. Atmos. 108, 4183.

Boylan, J.W., Russell, A.G., 2006. PM and light extinction model performance metrics, goals, and criteria for three-dimensional air quality models. Atmos. Environ. 40, 4946–4959.

Cao, L.M., Huang, X.F., Li, Y.Y., Hu, M., He, L.Y., 2018. Volatility measurement of atmospheric submicron aerosols in an urban atmosphere in southern China. Atmos. Chem. Phys. 18, 1729–1743.

Crippa, M., DeCarlo, P.F., Slowik, J.G., Mohr, C., Heringa, M.F., Chirico, R., Poulain, L., Freutel, F., Sciare, J., Cozic, J., DiMarco, C.F., Elsasser, M., Nicolas, J.B., Marchand, N., Abidi, E., Wiedensohler, A., Drewnick, F., Schneider, J., Borrmann, S., Nemitz, E., Zimmermann, R., Jaffrezo, J.-L., Prévôt, A.S.H., Baltensperger, U., 2013. Wintertime aerosol chemical composition and source apportionment of the organic fraction in the metropolitan area of Paris. Atmos. Chem. Phys. 13, 961–981.

Dobson, J.E., Bright, E.A., Coleman, P.R., Durfee, R.C., Worley, B.A., 2000. LandScan: a global population database for estimating populations at risk. Photogramm. Eng. Rem. Sens. 66, 849–857.

Elser, M., Huang, R.-J., Wolf, R., Slowik, J.G., Wang, Q., Canonaco, F., Li, G., Bozzetti, C., Daellenbach, K.R., Huang, Y., Zhang, R., Li, Z., Cao, J., Baltensperger, U., El-Haddad, I., Prévôt, A.S.H., 2016. New insights into $PM_{2.5}$ chemical composition and sources in two major cities in China during extreme haze events using aerosol mass spectrometry. Atmos. Chem. Phys. 16, 3207–3225.

Feng, T., Li, G., Cao, J., Bei, N., Shen, Z., Zhou, W., Liu, S., Zhang, T., Wang, Y., Huang, R.-J., Tie, X., Molina, L.T., 2016. Simulations of organic aerosol concentrations during springtime in the Guanzhong Basin, China. Atmos. Chem. Phys. 16, 10045–10061.

Fountoukis, C., Megaritis, A.G., Skyllakou, K., Charalampidis, P.E., Denier van der Gon, H.A.C., Crippa, M., Prévôt, A.S.H., Fachinger, F., Wiedensohler, A., Pilinis, C., Pandis, S.N., 2016. Simulating the formation of carbonaceous aerosol in a European Megacity (Paris) during the MEGAPOLI summer and winter campaigns. Atmos. Chem. Phys. 16, 3727–3741.

Fu, T.-M., Cao, J.J., Zhang, X.Y., Lee, S.C., Zhang, Q., Han, Y.M., Qu, W.J., Han, Z., Zhang, R., Wang, Y.X., Chen, D., Henze, D.K., 2012. Carbonaceous aerosols in China: top-down constraints on primary sources and estimation of secondary contribution. Atmos. Chem. Phys. 12, 2725–2746.

Guenther, A., Karl, T., Harley, P., Wiedinmyer, C., Palmer, P.I., Geron, C., 2006. Estimates of global terrestrial isoprene emissions using MEGAN (model of emissions of Gases and aerosols from nature). Atmos. Chem. Phys. 6, 3181–3210.

Guo, J.C., Zhou, S.S., Cai, M.F., Zhao, J., Song, W., Zhao, W.X., Hu, W.W., Sun, Y.L., He, Y., Yang, C.Q., Xu, X.Z., Zhang, Z.S., Cheng, P., Fan, Q., Hang, J., Fan, S.J., Wang, X.M., Wang, X.M., 2020. Characterization of submicron particles by time-of-flight aerosol chemical speciation monitor (ToF-ACSM) during wintertime: aerosol composition, sources, and chemical processes in Guangzhou, China. Atmos. Chem. Phys. 20, 7595–7615.

Hallquist, M., Wenger, J.C., Baltensperger, U., Rudich, Y., Simpson, D., Claeys, M., Dommen, J., Donahue, N.M., George, C., Goldstein, A.H., Hamilton, J.F., Herrmann, H., Hoffmann, T., Iinuma, Y., Jang, M., Jenkin, M.E., Jimenez, J.L., Kiendler-Scharr, A., Maenhaut, W., McFiggans, G., Mentel, ThF., Monod, A., Prévôt, A.S.H., Seinfeld, J.H., Surratt, J.D., Szmigielski, R., Wildt, J., 2009. The formation, properties and impact of secondary organic aerosol: current and emerging issues. Atmos. Chem. Phys. 9, 5155–5236.

He, L.Y., Hu, M., Huang, X.F., Yu, B.D., Zhang, Y.H., Liu, D.Q., 2004. Measurement of emissions of fine particulate organic matter from Chinese cooking. Atmos. Environ. 38, 6557–6564.

Horowitz, L.W., Walters, S., Mauzerall, D.L., Emmons, L.K., Rasch, P.J., Granier, C., Tie, X.X., Lamarque, J.F., Schultz, M.G., Tyndall, G.S., Orlando, J.J., Brasseur, G.P., 2003. A global simulation of tropospheric ozone and related tracers: description and evaluation of MOZART, version 2. J. Geophys. Res. Atmos. 108, 4784.

Hu, J., Wang, P., Ying, Q., Zhang, H., Chen, J., Ge, X., Li, X., Jiang, J., Wang, S., Zhang, J., Zhao, Y., Zhang, Y., 2017. Modeling biogenic and anthropogenic secondary organic aerosol in China. Atmos. Chem. Phys. 17, 77–92.

Hua, J.Y., Zhang, X.Y., Ren, C., Shi, Y., Lee, T.C., 2021. Spatiotemporal assessment of extreme heat risk for high-density cities: a case study of Hong Kong from 2006 to 2016. Sustain. Cities Soc. 64, 102507.

IPCC, 2013. Contribution of Working Groups I, II and III to the Fifth Assessment Report of the Intergovernmental Panel on Climate Change. https://archive.ipcc.ch/report/ar5/syr/.

Jimenez, J.L., Canagaratna, M.R., Donahue, N.M., Prévôt, A.S., Zhang, Q., Kroll, J.H., DeCarlo, P.F., Allan, J.D., Coe, H., Ng, N.L., Aiken, A.C., Docherty, K.S., Ulbrich, I. M., Grieshop, A.P., Robinson, A.L., Duplissy, J., Smith, J.D., Wilson, K.R., Lanz, V.A., Hueglin, C., Sun, Y.L., Tian, J., Laaksonen, A., Raatikainen, T., Rautiainen, J., Vaattovaara, P., Ehn, M., Kulmala, M., Tomlinson, J.M., Collins, D.R., Cubison, M.J., Dunlea, E.J., Huffman, J.A., Onasch, T.B., Alfarra, M.R., Williams, P.I., Bower, K., Kondo, Y., Schneider, J., Drewnick, F., Borrmann, S., Weimer, S., Demerjian, K., Salcedo, D., Cottrell, L., Griffin, R., Takami, A., Miyoshi, T., Hatakeyama, S., Shimono, A., Sun, J.Y., Zhang, Y.M., Dzepina, K., Kimmel, J.R., Sueper, D., Jayne, J. T., Herndon, S.C., Trimborn, A.M., Williams, L.R., Wood, E.C., Middlebrook, A.M., Kolb, C.E., Baltensperger, U., 2009. Worsnop, D. R. Evolution of organic aerosols in the atmosphere. Science 326 (5959), 1525–1529.

Katz, E.F., Guo, H.Y., Campuzano-Jost, P., Day, D.A., Brown, W.L., Boedicker, E., Pothier, M., Lunderberg, D.M., Patel, S., Patel, K., Hayes, P.L., Avery, A., Ruiz, L.H., Goldstein, A.H., Vance, M.E., Farmer, D.K., Jimenez, J.L., DeCarlo, P.F., 2021. Quantification of cooking organic aerosol in the indoor environment using aerodyne aerosol mass spectrometers. Aerosol Sci. Technol. https://doi.org/10.1080/02786826.2021.1931013.

Lee, B.P., Li, Y.J., Yu, J.Z., Louie, P.K.K., Chan, C.K., 2015. Characteristics of submicron particulate matter at the urban roadside in downtown Hong Kong—overview of 4 months of continuous high-resolution aerosol mass spectrometer measurements. J. Geophys. Res. Atmos. 120, 7040–7058.

Li, G., Zavala, M., Lei, W., Tsimpidi, A.P., Karydis, V.A., Pandis, S.N., Canagaratna, M.R., Molina, L.T., 2011. Simulations of organic aerosol concentrations in Mexico City using the WRF-CHEM model during the MCMA-2006/MILAGRO campaign. Atmos. Chem. Phys. 11, 3789–3809.

Li, N., Fu, T.-M., Cao, J., Lee, S., Huang, X.-F., He, L.-Y., Ho, K.-F., Fu, J.S., Lam, Y.-F., 2013. Sources of secondary organic aerosols in the Pearl River Delta region in fall: contributions from the aqueous reactive uptake of dicarbonyls. Atmos. Environ. 76, 200–207.

Liu, T.Y., Li, Z.J., Chan, M.N., Chan, C.K., 2017. Formation of secondary organic aerosols from gas-phase emissions of heated cooking oils. Atmos. Chem. Phys. 17, 7333–7344.

Liu, T.Y., Wang, Z.Y., Wang, X.M., Chan, C.K., 2018a. Primary and secondary organic aerosol from heated cooking oil emissions. Atmos. Chem. Phys. 18, 11363–11374.

Liu, T.Y., Wang, Z.Y., Huang, D.D., Wang, X.M., Chan, C.K., 2018b. Significant production of secondary organic aerosol from emissions of heated cooking oils. Environ. Sci. Technol. Lett. 5, 32–37.

Liu, T.Y., Zhou, L.Y., Liu, Q.Y., Lee, B.P., Yao, D.W., Lu, H.X., Lyu, X.P., Guo, H., Chan, C. K., 2019. Secondary organic aerosol formation from urban roadside air in Hong Kong. Environ. Sci. Technol. 53, 3001–3009.

Louvaris, E.E., Karnezi, E., Kostenidou, E., Kaltsonoudis, C., Pandis, S.N., 2017. Estimation of the volatility distribution of organic aerosol combining thermodenuder and isothermal dilution measurements. Atmos. Meas. Tech. 10, 3909–3918.

Miao, R.Q., Chen, Q., Zheng, Y., Cheng, X., Sun, Y.L., Palmer, P.I., Shrivastava, M., Guo, J.P., Zhang, Q., Liu, Y.H., Tan, Z.F., Ma, X.F., Chen, S.Y., Zeng, L.M., Lu, K.D., Zhang, Y.H., 2020. Model bias in simulating major chemical components of $PM_{2.5}$ in China. Atmos. Chem. Phys. 20, 12265–12284.

Mohr, C., DeCarlo, P.F., Heringa, M.F., Chirico, R., Slowik, J.G., Richter, R., Reche, C., Alastuey, A., Querol, X., Seco, R., Peñuelas, J., Jiménez, J.L., Crippa, M., Zimmermann, R., Baltensperger, U., Prévôt, A.S.H., 2012. Identification and quantification of organic aerosol from cooking and other sources in Barcelona using aerosol mass spectrometer data. Atmos. Chem. Phys. 12, 1649–1665.

Ots, R., Vieno, M., Allan, J.D., Reis, S., Nemitz, E., Young, D.E., Coe, H., Marco, C.D., Detournay, A., Mackenzie, I.A., Green, D.C., Heal, M.R., 2016. Model simulations of cooking organic aerosol (COA) over the UK using estimates of emissions based on measurements at two sites in London. Atmos. Chem. Phys. 16, 13773–13789.

Qin, Y.M., Tan, H.B., Li, Y.J., Schurman, M.I., Li, F., Canonaco, F., Prévôt, A.S.H., Chak, C.K., 2017. Impacts of traffic emissions on atmospheric particulate nitrate and organics at a downwind site on the periphery of Guangzhou, China. Atmos. Chem. Phys. 17, 10245–10258.

Reyes-Villegas, E., Bannan, T., Le Breton, M., Mehra, A., Priestley, M., Percival, C., Coe, H., Allan, J.D., 2018. Online chemical characterization of food-cooking organic aerosols: implications for source apportionment. Environ. Sci. Technol. 52, 5308–5318, 2018.

Sun, Y.L., Xu, W.Q., Zhang, Q., Jiang, Q., Canonaco, F., Prévôt, A.S.H., Fu, P.Q., Li, J., Jayne, J., Worsnop, D.R., Wang, Z.F., 2018. Source apportionment of organic aerosol from 2-year highly time-resolved measurements by an aerosol chemical speciation monitor in Beijing, China. Atmos. Chem. Phys. 18, 8469–8489.

Sun, Y.L., Zhang, Q., Schwab, J.J., Demerjian, K.L., Chen, W.N., Bae, M.S., Hung, H.M., Hogrefe, O., Frank, B., Rattigan, O.V., Lin, Y.C., 2011. Characterization of the sources and processes of organic and inorganic aerosols in New York city with a high-resolution time-of-flight aerosol mass apectrometer. Atmos. Chem. Phys. 11, 1581–1602.

Takhar, M., Li, Y.C., Chan, A.W.H., 2021. Characterization of secondary organic aerosol from heated-cooking-oil emissions: evolution in composition and volatility. Atmos. Chem. Phys. 21, 5137–5149.

Takhar, M., Stroud, C.A., Chan, A.W.H., 2019. Volatility distribution and evaporation rates of organic aerosol from cooking oils and their evolution upon heterogeneous oxidation. ACS Earth Space Chem. 3, 1717–1728.

Tsimpidi, A.P., Karydis, V.A., Zavala, M., Lei, W., Molina, L., Ulbrich, I.M., Jimenez, J.L., Pandis, S.N., 2010. Evaluation of the volatility basis-set approach for the simulation of organic aerosol formation in the Mexico City metropolitan area. Atmos. Chem. Phys. 10, 525–546.

Wang, L.N., Xiang, Z.Y., Stevanovic, S., Ristovski, Z., Salimi, F., Gao, J., Wang, H.L., Li, L., 2017. Role of Chinese cooking emissions on ambient air quality and human health. Sci. Total Environ. 589, 173–181.

Wiedinmyer, C., Quayle, B., Geron, C., Belote, A., McKenzie, D., Zhang, X., O'Neill, S., Wynne, K.K., 2006. Estimating emissions from fires in North America for air quality modeling. Atmos. Environ. 40, 3419–3432.

Wiedinmyer, C., Akagi, S.K., Yokelson, R.J., Emmons, L.K., Al-Saadi, J.A., Orlando, J.J., Soja, A.J., 2011. The Fire INventory from NCAR (FINN): a high resolution global model to estimate the emissions from open burning. Geosci. Model Dev. (GMD) 4, 625–641.

Xing, L., Fu, T.M., Cao, J.J., Lee, S.C., Wang, G.H., Ho, K.F., Cheng, M.C., You, C.F., Wang, T.J., 2013. Seasonal and spatial variability of the OM/OC mass ratios and high regional correlation between oxalic acid and zinc in Chinese urban organic aerosols. Atmos. Chem. Phys. 13, 4307–4318.

Xing, L., Li, G.H., Pongpiachan, S., Wang, Q.Y., Han, Y.M., Cao, J.J., Tipmanee, D., Palakun, J., Aukkaravittayapun, S., Surapipith, V., Poshyachinda, S., 2020. Quantifying the contributions of local emissions and regional transport to elemental carbon in Thailand. Environ. Pollut. 262, 114272.

Xing, L., Wu, J.R., Elser, M., Tong, S.R., Liu, S.X., Li, X., Liu, L., Cao, J., Zhou, J.M., El-Haddad, I., Huang, R.J., Ge, M.F., Tie, X.X., Prévôt, A.S.H., Li, G.H., 2019. Wintertime secondary organic aerosol formation in Beijing–Tianjin–Hebei (BTH):

contributions of HONO sources and heterogeneous reactions. Atmos. Chem. Phys. 19, 2343–2359.
Xu, L., Suresh, S., Guo, H., Weber, R.J., Ng, N.L., 2015. Aerosol characterization over the southeastern United States using high-resolution aerosol mass spectrometry: spatial and seasonal variation of aerosol composition and sources with a focus on organic nitrates. Atmos. Chem. Phys. 15, 7307–7336.
Yan, D.H., Wu, S.H., Zhou, S.L., Tong, G.J., Li, F.F., Wang, Y.M., Li, B.J., 2019. Characteristics, sources and health risk assessment of airborne particulate PAHs in Chinese cities: a review. Environ. Pollut. 248, 804–814.
Yao, D.W., Lyu, X.P., Lu, H.X., Zeng, L.W., Liu, T.Y., Chan, C.K., Guo, H., 2021. Characteristics, sources and evolution processes of atmospheric organic aerosols at a roadside site in Hong Kong. Atmos. Environ. 252, 118298.
Ye, T.T., Zhao, N.Z., Yang, X.C., Ouyang, Z.T., Liu, X.P., Chen, Q., Hu, K.J., Yue, W.Z., Qi, J.G., Li, Z.S., Jia, P., 2019. Improved population mapping for China using remotely sensed and points-of-interest data within a random forests model. Sci. Total Environ. 658, 936–946.
Zhai, S.X., Jacob, D.J., Wang, X., Shen, L., Li, K., Zhang, Y.Z., Gui, K., Zhao, T.L., Liao, H., 2019. Fine particulate matter ($PM_{2.5}$) trends in China, 2013–2018: separating contributions from anthropogenic emissions and meteorology. Atmos. Chem. Phys. 19, 11031–11041.
Zhang, Q., Jimenez, J.L., Canagaratna, M.R., Allan, J.D., Coe, H., Ulbrich, I., Alfarra, M. R., Takami, A., Middlebrook, A.M., Sun, Y.L., Dzepina, K., Dunlea, E., Docherty, K., De- Carlo, P.F., Salcedo, D., Onasch, T., Jayne, J.T., Miyoshi, T., Shimono, A., Hatakeyama, S., Takegawa, N., Kondo, Y., Schneider, J., Drewnick, F., Borrmann, S., Weimer, S., Demerjian, K., Williams, P., Bower, K., Bahreini, R., Cottrell, L., Griffin, R.J., Rautiainen, J., Sun, J.Y., Zhang, Y.M., Worsnop, D.R., 2007. Ubiquity and dominance of oxygenated species in organic aerosols in anthropogenically-influenced Northern Hemisphere midlatitudes. Geophys. Res. Lett. 34, L13801.
Zhang, Q., Jimenez, J.L., Canagaratna, M.R., Ulbrich, I.M., Ng, N.L., Worsnop, D.R., Sun, Y.L., 2011. Understanding atmospheric organic aerosols via factor analysis of aerosol mass spectrometry: a review. Anal. Bioanal. Chem. 401, 3045–3067.
Zhang, Q., Streets, D.G., Carmichael, G.R., He, K.B., Huo, H., Kannari, A., Klimont, Z., Park, I.S., Reddy, S., Fu, J.S., Chen, D., Duan, L., Lei, Y., Wang, L.T., Yao, Z.L., 2009. Asian emissions in 2006 for the NASA INTEX-B mission. Atmos. Chem. Phys. 9, 5131–5153.
Zhang, Z.R., Zhu, W.F., Hu, M., Wang, H., Chen, Z., Shen, R.Z., Yu, Y., Tan, R., Guo, S., 2020. Secondary organic aerosol from typical Chinese domestic cooking emissions. Environ. Sci. Technol. Lett. 8, 24–31.
Zheng, B., Tong, D., Li, M., Liu, F., Hong, C.P., Geng, G.N., Li, H.Y., Li, X., Peng, L.Q., Qi, J., Yan, L., Zhang, Y.X., Zhao, H.Y., Zheng, Y.X., He, K.B., Zhang, Q., 2018. Trends in China's anthropogenic emissions since 2010 as the consequence of clean air actions. Atmos. Chem. Phys. 18, 14095–14111.
Zhou, W., Xu, W.Q., Kim, H., Zhang, Q., Fu, P.Q., Worsnop, D.R., Sun, Y.L., 2020. A review of aerosol chemistry in Asia: insights from aerosol mass spectrometer measurements. Environ. Sci.: Processes Impacts. 22, 1616–1653.